



## Solid-phase extraction and separation of Brilliant Green by Fe<sub>3</sub>O<sub>4</sub> magnetic nano-particles functionalized by sodium dodecyl sulphate from aqueous solution: multivariate optimization and adsorption characterization

Javad Zolgharnein\*, Shahab Feshki

Department of Chemistry, Faculty of Science, Arak University, Arak 38156-8-8394, Iran, Tel. +98 8634173401;  
Fax: +98 863 4173406; emails: J-zolgharnein@araku.ac.ir, J.zolgharnein@gmail.com (J. Zolgharnein)

Received 24 August 2016; Accepted 18 March 2017

### ABSTRACT

Fe<sub>3</sub>O<sub>4</sub> magnetic nano-particles functionalized by sodium dodecyl sulphate (SDS) were used for separation and efficient removal of Brilliant Green (BG) dye from aqueous solutions in a batch system. Adsorption process of dye was optimized by means of a multivariate approach, such as response surface methodology. Box–Behnken design was performed to evaluate the influences of various experimental factors for instance: pH, adsorbent dose (*m*) and initial dye concentration (*C<sub>d</sub>*), on the removal percent (*R*%) and uptake capacity (*q*). The optimum conditions for BG adsorption by nano-Fe<sub>3</sub>O<sub>4</sub>-SDS were found to be: pH = 4; nano-Fe<sub>3</sub>O<sub>4</sub> = 8 mg; SDS = 10.8 mg and *C<sub>d</sub>* = 600 mg /L. Simultaneous optimization of both responses *R*% and uptake capacity (*q*) was also performed through applying a desirability function approach. The results obtained for simultaneous optimization of *R*% = 64 and *q* = 440 mg/g with 99% overall desirability (*D* = 0.99) are: pH = 4; *C<sub>d</sub>* = 600 mg/L; nano-Fe<sub>3</sub>O<sub>4</sub> = 8.8 mg and SDS = 10.9 mg. Under optimum conditions, pre-concentration of water sample was achieved by containing BG with the enrichment factor of 63 and DL = 3.0 µg/L and RSD = 2.1% (*n* = 9) for 21.14 µg/L. Isotherm modelling and thermodynamic studies for further information about BG behaviour with nano-Fe<sub>3</sub>O<sub>4</sub>-SDS adsorbent were investigated. The morphology and properties of the magnetite nano-particles produced was determined by scanning electron microscopy, X-ray diffraction, vibrating sample magnetometer, Fourier transform infrared spectroscopy and thermogravimetric analysis. As a result of this study, functionalizing Fe<sub>3</sub>O<sub>4</sub> magnetic nano-particles considerably improved the efficiency of the adsorption process of BG.

*Keywords:* Adsorption; Brilliant Green; Box–Behnken design; magnetic nano-particles; Sodium dodecyl sulphate

### 1. Introduction

Dyes used in industries such as paper printing and textile colouring generate serious concerns for the environment and biota [1–7]. It is known that significant amount of the total world production of dyes is wasted during the dyeing process and is disposed as effluents [2–4]. Discharging dyes into water resources is quite unfavourable, since water quality, its physical, and chemical and biological properties dramatically change [3–5]. Alongside its colouring function

as biological stain, Brilliant Green (BG) is used with medical and clinical applications [5–7]. However, most of the applied dyes used in paper printing, textile industries and clinical use generate serious health concerns for organisms, humans and the environment [7]. Knowing that most dyes are not degradable or removable through the ordinary treatment processes, new approaches are increasingly sought by researchers [1–8]. Among dye-removal techniques, adsorption has a unique features, due to its several advantages: for instance, simplicity, high efficiency, and being an inexpensive and environmentally friendly method [8]. It is an equilibrium-based process which has flexibility, easily designable, and also involves relatively simple operational

\* Corresponding author.

characteristics [8]. Since the development of an adsorption process requires a new proper adsorbent, which enhances efficiency, selectivity and value for money, researchers have been stimulated to design and prepare a new class of adsorbents [1–8]. In recent decades, beyond the conventional and low-cost adsorbents [1–9], a new class of nano-sized materials has been developed [10–17]. Among the nano-particles material especially nano-oxides (e.g.,  $\text{Fe}_2\text{O}_3$ ,  $\text{Fe}_3\text{O}_4$ ,  $\text{TiO}_2$ ,  $\text{SiO}_2$ ,  $\text{Al}_2\text{O}_3$ ,  $\text{MgO}$ ,  $\text{CeO}_2$  and Fe–Zn bimetallic nano-particles), magnetic nano-particles have several advantages over the conventional nano-sized adsorbents [10–19]. Not only they have a high surface area, which can impart a higher adsorption capacity, but also they possess powerful superparamagnetic properties that lead to rapid extraction–separation by employing a strong external magnetic field [10–19]. Thus, it is used as a novel adsorbent for the pre-concentration of an analyte from large-volume samples in the solid-phase extraction (SPE) method used for the separation, elimination and determination of chemical species [16–23]. Several research studies have been published on the application of a variety of nano-magnetic particles for the treatment and remediation of pollutants in the environment [10–30]. However, nano-oxide adsorbents, besides their several benefits, have limitations such as low selectivity, affinity and efficiency, in relation to several various pollutants [16,17,25,26]. In order to overcome these problems the functionalization and modification of nano-oxides as new adsorbents is reported as a new invention [16,22–28]. Surfactants are among the various compounds that have been widely used for enhancing and improving both affinity and efficiency of adsorbents in adsorption process [16,22–33]. The head group of surfactants (both cationic and anionic forms) appear via an electrostatic attraction adsorbed on a charged nano-oxide surface through a well-known admicelles and hemimicelles formation mechanism, as described previously [16,29–33]. In this study nano- $\text{Fe}_3\text{O}_4$ , which has a high surface area and strong magnetic property, is functionalized by sodium dodecyl sulphate (SDS). It is employed to improve the adsorption capacity and its affinity and selectivity towards dyes, and eludes the time-consuming enrichment process of loading large-volume samples through the rapid isolation of  $\text{Fe}_3\text{O}_4$  with an external magnet [10–24]. The capability of adsorbents to remove pollutants is forcefully influenced by some factors, such as initial pH, initial concentration of the pollutant and sorbent amount. Multivariate optimization through response surface methodology (RSM) due to its several benefits, rather than using the “one-at-the-time” method is implied to investigate the influential effects of factors, modelling them with responses ( $R\%$ : removal percent and  $q$ : uptake capacity) and finding optimum adsorption and SPE conditions [4,6,23,25,26]. However, the main goal of this study is to functionalize nano- $\text{Fe}_3\text{O}_4$  through SDS (nano- $\text{Fe}_3\text{O}_4$ -SDS) as a new efficient adsorbent for pre-concentration, and the removal of BG from aqueous solutions [27–33]. The Box–Behnken design (BBD), as a multivariate optimization approach, is applied for the adsorption process of BG; it also enables visualization by means of responses showing effective factors, interactions and the yielding of optimum conditions. The adsorptive behaviour of nano- $\text{Fe}_3\text{O}_4$ -SDS by several surface analysis techniques was investigated, such as X-ray diffraction (XRD), scanning electron microscopy (SEM), along with Fourier

transform infrared (FT-IR) spectroscopy, thermogravimetric analysis (TGA) and vibrating sample magnetometer (VSM). Isotherms and thermodynamics studies of the adsorption of BG onto nano- $\text{Fe}_3\text{O}_4$ -SDS, were also scrutinized.

## 2. Materials and methods

### 2.1. Materials

$\text{FeCl}_2 \cdot 4\text{H}_2\text{O}$  and  $\text{FeCl}_3 \cdot 6\text{H}_2\text{O}$  were purchased from Merck (Darmstadt, Germany). The anionic surfactant SDS, BG dye (chemical formula =  $\text{C}_{27}\text{H}_{34}\text{N}_2\text{O}_4\text{S}$ , FW = 482.62) was purchased from Merck (Darmstadt, Germany; Fig. 1). An accurately weighed quantity of the dye was dissolved in double-distilled water to prepare a stock solution (1,000 mg/L). Experimental solutions of the desired concentrations were obtained by successive dilutions with double-distilled water.

### 2.2. Preparation of magnetic ( $\text{Fe}_3\text{O}_4$ ) nano-particles

$\text{Fe}_3\text{O}_4$  nano-particles were prepared by mixing  $\text{FeCl}_2 \cdot 4\text{H}_2\text{O}$  (2.0 g),  $\text{FeCl}_3 \cdot 6\text{H}_2\text{O}$  (5.2 g) and 0.85 mL hydrochloric acid in 25 mL of deionized water, degassed with nitrogen beforehand. This mixture was added to a stirred 250 mL NaOH solution (1.5 M), while nitrogen gas was passed continuously through the solution during the reaction [13,19,28,34]. The produced magnetic nano-particles were rinsed with deionized water (three times with 150 mL) and then resuspended in deionized water (250 mL). The generated magnetic nano-particles concentration was estimated to be about 10 mg/mL. Further, the magnetic nano-particles were characterized.

### 2.3. Characterization techniques

The FT-IR is used to record the spectra of the adsorbent in the range of  $400\text{--}4,000\text{ cm}^{-1}$  by means of a UNICAM-Galaxy series FT-IR 5000 and to identify functional groups of adsorbents. In addition, XRD pattern of the sorbent was recorded using a Philips X-ray diffractometer XRD spectrum Bruker D8 Advance. The XRD measurements were made over a range of  $30^\circ\text{--}50^\circ$ , using a Phillips powder diffractometer model PW3040 with Cu  $K\alpha$  radiation at a scan speed of  $1^\circ/\text{min}$ . The surface morphology of magnetic  $\text{Fe}_3\text{O}_4$  nano-particles was imaged using SEM (VEGA \ \TESCAN). The scanning was performed at an accelerating voltage of 20 Kv. TGA was

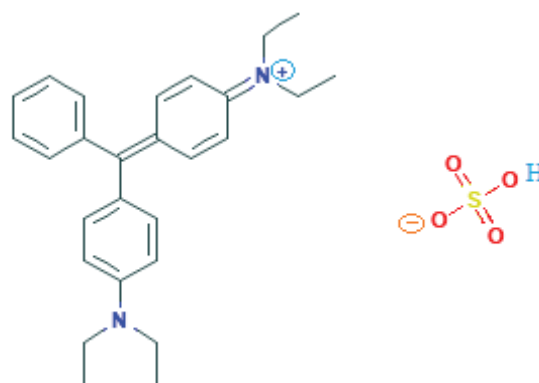


Fig. 1. Molecular structure of Brilliant Green.

carried out with a thermogravimetric analyzer (NETZSCH TG 209 F1). The magnetization plots of samples were measured with a VSM (VSM 3886 Kashan, Iran).

#### 2.4. Batch experiment

All experimental considerations of adsorptive removal of BG with magnetic nano-particles functionalized by SDS (nano-Fe<sub>3</sub>O<sub>4</sub>-SDS) were conducted as batch experiments at room temperature. In a typical run, 25 mL of the fresh BG solution was used, and a planned amount of sorbent (Tables 1 and 2) was added to each sample solution. The pH of the solution was adjusted with HCl or NaOH (Metrohm, model 744) before adding the sorbent. The mixture was

Table 1  
Factors and their levels used in the BBD design

| Factors                                       | -1.00 | 0.00 | 1.00 |
|---|-------|------|------|
| SDS (S), mg/L                                 | 0.1   | 0.6  | 1.1  |
| Nano-Fe <sub>3</sub> O <sub>4</sub> (N), mg/L | 0.2   | 1.1  | 2    |
| pH  | 4     | 5.5  | 7    |
| CBG (C <sub>d</sub> ), mg/L                   | 100   | 350  | 600  |

Table 2  
BBD design and results obtained for both adsorption responses R% and q

| Number run | S   | N   | pH  | C <sub>d</sub> (mg/L) | R%    | q     |
|------------|-----|-----|-----|-----------------------|-------|-------|
| 1          | 0.1 | 0.2 | 5.5 | 350                   | 16.0  | 466.7 |
| 2          | 1.1 | 0.2 | 5.5 | 350                   | 57.0  | 356.2 |
| 3          | 0.1 | 2.0 | 5.5 | 350                   | 55.0  | 229.2 |
| 4          | 1.1 | 2.0 | 5.5 | 350                   | 79.0  | 216.1 |
| 5          | 0.6 | 1.1 | 4.0 | 100                   | 89.0  | 127.1 |
| 6          | 0.6 | 1.1 | 7.0 | 100                   | 65.0  | 92.9  |
| 7          | 0.6 | 1.1 | 4.0 | 600                   | 48.0  | 411.4 |
| 8          | 0.6 | 1.1 | 7.0 | 600                   | 31.0  | 265.7 |
| 9          | 0.1 | 1.1 | 5.5 | 100                   | 62.0  | 129.2 |
| 10         | 1.1 | 1.1 | 5.5 | 100                   | 92.0  | 100.0 |
| 11         | 0.1 | 1.1 | 5.5 | 600                   | 32.0  | 400.0 |
| 12         | 1.1 | 1.1 | 5.5 | 600                   | 53.0  | 345.6 |
| 13         | 0.6 | 0.2 | 4.0 | 350                   | 43.0  | 442.6 |
| 14         | 0.6 | 2.0 | 4.0 | 350                   | 74.0  | 244.3 |
| 15         | 0.6 | 0.2 | 7.0 | 350                   | 29.0  | 298.5 |
| 16         | 0.6 | 2.0 | 7.0 | 350                   | 50.0  | 165.1 |
| 17         | 0.1 | 1.1 | 4.0 | 350                   | 42.9  | 312.8 |
| 18         | 1.1 | 1.1 | 4.0 | 350                   | 85.0  | 323.4 |
| 19         | 0.1 | 1.1 | 7.0 | 350                   | 37.4  | 272.7 |
| 20         | 1.1 | 1.1 | 7.0 | 350                   | 50.0  | 190.2 |
| 21         | 0.6 | 0.2 | 5.5 | 100                   | 61.0  | 179.4 |
| 22         | 0.6 | 2.0 | 5.5 | 100                   | 92.0  | 86.8  |
| 23         | 0.6 | 0.2 | 5.5 | 600                   | 27.7  | 488.9 |
| 24         | 0.6 | 2.0 | 5.5 | 600                   | 46.9  | 265.7 |
| 25         | 0.6 | 1.1 | 5.5 | 350                   | 59.4  | 297.0 |
| 26         | 0.6 | 1.1 | 5.5 | 350                   | 60.5  | 302.5 |
| 27         | 0.6 | 1.1 | 5.5 | 350                   | 60.50 | 302.5 |

stirred at 300 rpm, at a known temperature, for 5 min and collected by an external magnetic field.

#### 2.5. Analytical measurement

The concentration of the remaining BG dye in the solution was determined by finding the absorbance at the characteristic wavelength using a UV-visible spectrophotometer (Analytik Jena SPECORD 250, Germany). Standard solutions of the dye were taken, and the absorbance was determined at wavelength  $\lambda_{\max} = 629$  nm, and its calibration plot was obtained ( $y = 0.125x - 0.009$ ,  $R^2 = 0.9990$ ,  $x$  (mg/L)), which showed a linear range from 0.5 up to 15 mg/L concentration. However, the dye removal and equilibrium adsorption capacity ( $q$ ) was determined according to Eqs. (1) and (2), respectively:

$$\%R = \frac{(C_0 - C_e)}{C_0} \times 100 \quad (1)$$

$$q = \frac{(C_0 - C_e)}{m} \times V \quad (2)$$

where  $C_0$  is the BG initial concentration (mg/L);  $C_e$  is the equilibrium dye concentration (mg/L);  $V$  is the volume of solution (L); and  $m$  is the sorbent mass (g).

#### 2.6. Multivariate optimization via response surface methodology

The RSM is an efficient method for optimizing the adsorption process for a multivariable approach with a minimum number of experiments using a set of designed experiments [35,36]. The BBD is among RSM, which is a spherical, rotatable or nearly rotatable second-order design. It is based on a three-level incomplete factorial design, which consists of a centre point and middle point of the edges from a cube. The number of experimental points is defined by the expression  $N = 2k(k - 1) + C_0$ , where  $k$  is the number of variables, and  $C_0$  is the number of centre points [35–38]. The most significant advantage of the BBD matrix is to avoid experiments performed under extreme conditions, for which unsatisfactory results may occur [17,25,35–38].

However, BBD leads to a second-order model explaining the adsorption responses ( $R\%$  and  $q$ ) through applying a multiple regression analysis to the experimental data [17,25,37,38].

$$y = \beta_0 + \sum_{i=1}^k \beta_i x_i + \sum_{i=1}^k \beta_{ii} x_i^2 + \sum_{i=1}^{k-1} \sum_{j=2}^k \beta_{ij} x_i x_j + \varepsilon \quad (3)$$

where  $x_1, x_2, \dots, x_k$  are the input factors that influence the response  $y$ ;  $\beta_0$  is a constant;  $\beta_i$  is the slope or linear effect of the input factor  $x_i$ ;  $\beta_{ii}$  is the quadratic effect of the input factor  $x_i$  ( $i = 1, 2, \dots, k$ );  $\beta_{ij}$  is the linear by linear interaction effect between the input factors  $x_i$  and  $x_j$  ( $i = 1, 2, \dots, k$ ;  $j = 1, 2, \dots, k$ ) are unknown parameters; and  $\varepsilon$  is a random error. The  $\beta$  coefficients, which should be determined in the second-order model, are obtained by the least square method [33–36]. The MINITAB 17 statistical software was used for regression analysis of the obtained data and to estimate the coefficient

of regression equation. In the present study, by employing the BBD, the effect of the three independent variables on the removal percent ( $R\%$ ) and uptake capacity ( $q$ ) was investigated.

### 3. Results and discussion

#### 3.1. Effect of SDS

It is observed that magnetic nano-particles ( $\text{Fe}_3\text{O}_4$ ) cannot adsorb BG from an aqueous solution at all, while its SDS modified form adsorbed BG efficiently (Fig. 2). The effect of SDS modified magnetite nano-particles ( $\text{Fe}_3\text{O}_4$ ) on the adsorption of BG was shown for the removal of BG in a 25.0 mL of 100.0 mg/L BG solution at pH = 4 in Fig. 2. The surfaces of metal oxides ( $\text{Fe}_3\text{O}_4$  suspension) are generally covered by sulphate groups of SDS that vary its forms at different pHs. The adsorbent surface below the pH of zero point charge ( $\text{pH}_{\text{zpc}}$  is around 6.5 for nano- $\text{Fe}_3\text{O}_4$ -SDS) is positively charged and hydrophilic, while beyond this point it became negatively charged. Therefore, the adsorption of BG, which is a cationic dye (Fig. 1), onto the magnetic nano-particles ( $\text{Fe}_3\text{O}_4$ ) does not take place (Fig. 2(a)). At a lower pH ( $\approx 4$ ), an anionic surfactant, such as SDS molecules, will be adsorbed onto the surface of nano- $\text{Fe}_3\text{O}_4$  through an electrostatic attraction (Coulombic attraction) between negative and positive heads, and make the surface of adsorbent hydrophobic. Thus the monolayer adsorbed surfactant called hemimicelles can be formed. Functionalizing of nano- $\text{Fe}_3\text{O}_4$  by SDS also increases the stability of nano- $\text{Fe}_3\text{O}_4$  at pH = 4. As a result, the dye is trapped into the hydrophobic tails of hemimicelles of modified adsorbent (Fig. 3(b)) [23,25,26,30–32]. The effect of surface modification on the removal of BG is shown in Fig. 3, revealing that the removal percent of BG by nano- $\text{Fe}_3\text{O}_4$  is 6%, while removal by SDS is improved up to a very high value (96%), as a result of its functionalization.

#### 3.2. Structural characterization of nano- $\text{Fe}_3\text{O}_4$ -SDS

##### 3.2.1. FT-IR analysis

The FT-IR spectra of BG, nano- $\text{Fe}_3\text{O}_4$  and nano- $\text{Fe}_3\text{O}_4$ -SDS were taken before and after BG loading in a range of 400–4,000  $\text{cm}^{-1}$ , as shown in Figs. 4(a)–(c). In the case of nano- $\text{Fe}_3\text{O}_4$ , the broad absorption band at 3,340  $\text{cm}^{-1}$  indicates the presence of surface hydroxyl groups (O–H stretching) and the bands at low wave numbers ( $\leq 700 \text{ cm}^{-1}$ ) are related to vibrations of the Fe–O bonds in  $\text{Fe}_3\text{O}_4$  [17,19,24,39–42]. The phase identification nano- $\text{Fe}_3\text{O}_4$  can also be proven by the appearance of two strong absorption bands around 567.23 and 399.31  $\text{cm}^{-1}$  (Fig. 4(a)) [17,24,39–42]. In Fig. 4(b), SDS peaks at 2,920.41 and 2,853.54  $\text{cm}^{-1}$  due to the C–H stretching vibrations of CH,  $\text{CH}_2$  and  $\text{CH}_3$  groups. The additional bands in Fig. 4(b) reveal the coating of nano- $\text{Fe}_3\text{O}_4$  with SDS. The comparison of spectra in Fig. 4 shows that some peaks are changed and new peaks are created. For example, the stretching vibration of OH group shifted from 3,440 to 3,444  $\text{cm}^{-1}$  in the dye-loaded nano- $\text{Fe}_3\text{O}_4$ -SDS. A remarkable change occurs in the fingerprint region of the spectra that shows different patterns for unloaded (b) and loaded adsorbents (d). These results clarified how chemical interactions between the dye and the sorbent hydroxyl groups occur on the surface. This comparison also shows the

changing and shifting of many bands (for Fe–O: from 567 to 615  $\text{cm}^{-1}$ ), which confirms that functional groups presented in the nano- $\text{Fe}_3\text{O}_4$ -SDS are involved with BG during the adsorption process [17,19,24,28,39–42]. However, the FT-IR analyses confirmed that the SDS was successfully coated on the surface of nano- $\text{Fe}_3\text{O}_4$ .

##### 3.2.2. XRD, SEM and VSM analysis

In the XRD patterns, the peaks, positions and relative intensities for both nano- $\text{Fe}_3\text{O}_4$  and nano- $\text{Fe}_3\text{O}_4$ -SDS are shown in Fig. 5. Comparative analysis of XRD patterns indicates very distinguishable peaks for fine magnetite crystals, which means that these particles have phase stability [19,28,40]. SEM images depict the surface of nano- $\text{Fe}_3\text{O}_4$  (Fig. 6), which comprises nearly uniform mono-dispersed spheres. These spheres, with smooth surfaces, have a diameter of about 76–81 nm [17,19,42]. The magnetic properties of nano- $\text{Fe}_3\text{O}_4$  and nano- $\text{Fe}_3\text{O}_4$ -SDS show the hysteresis loops of superparamagnetic behaviour. As shown in

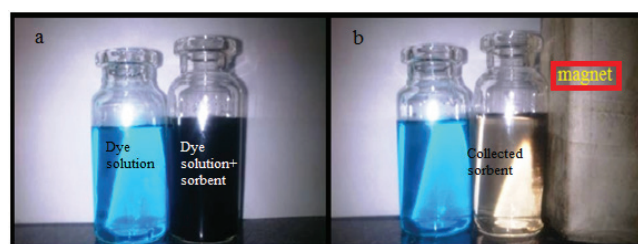


Fig. 2. Removal of Brilliant Green dye from the sample solution by nano- $\text{Fe}_3\text{O}_4$  (a) and nano- $\text{Fe}_3\text{O}_4$ -SDS (b).

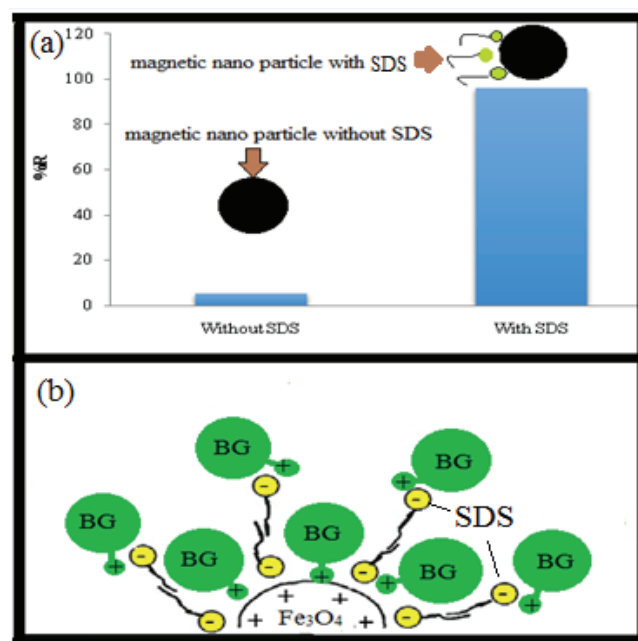


Fig. 3. Effect of SDS-modified magnetite nano-particles on adsorption of BG removal (25.0 mL of 100.0 mg/L BG solution at pH 4).

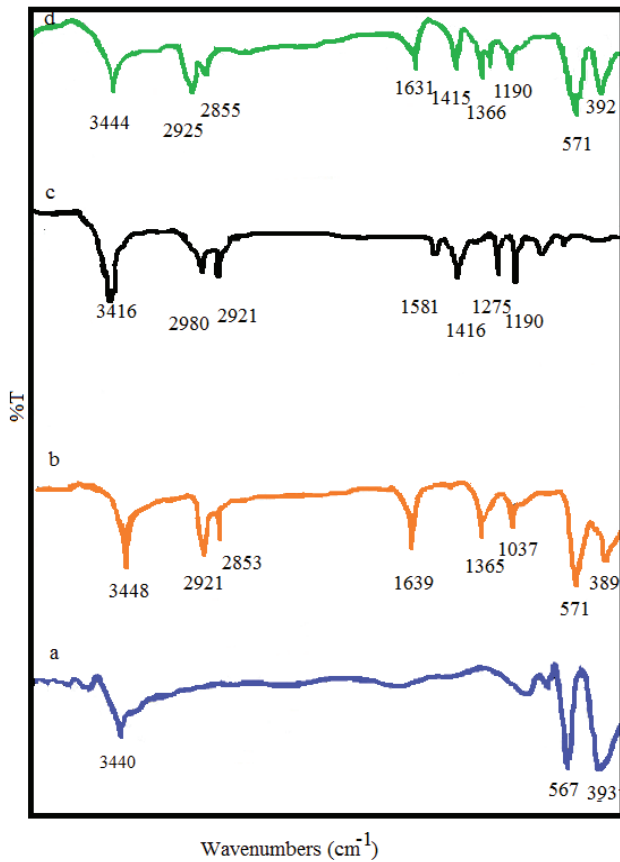


Fig. 4. FT-IR spectra of nano-Fe<sub>3</sub>O<sub>4</sub> (a), nano-Fe<sub>3</sub>O<sub>4</sub>-SDS before (b), BG dye (c), and after BG loading (d).

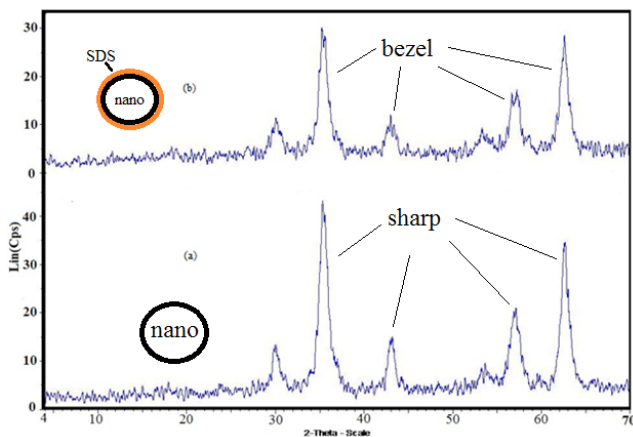


Fig. 5. Analysis of XRD patterns of both nano-Fe<sub>3</sub>O<sub>4</sub> (a) and nano-Fe<sub>3</sub>O<sub>4</sub>-SDS (b).

Fig. 7, the saturation magnetization values of nano-Fe<sub>3</sub>O<sub>4</sub> and nano-Fe<sub>3</sub>O<sub>4</sub>-SDS at high fields of up to  $\pm 8,500.0$  Oe and magnetic saturation (Ms) of samples are changed from 52.3 to 48.03 emu/g, respectively [19,24,42]. The results indicate that the prepared nano-Fe<sub>3</sub>O<sub>4</sub> were superparamagnetic, and this property did not significantly change when the SDS-coated nano-Fe<sub>3</sub>O<sub>4</sub> are separated from sample matrix by an external

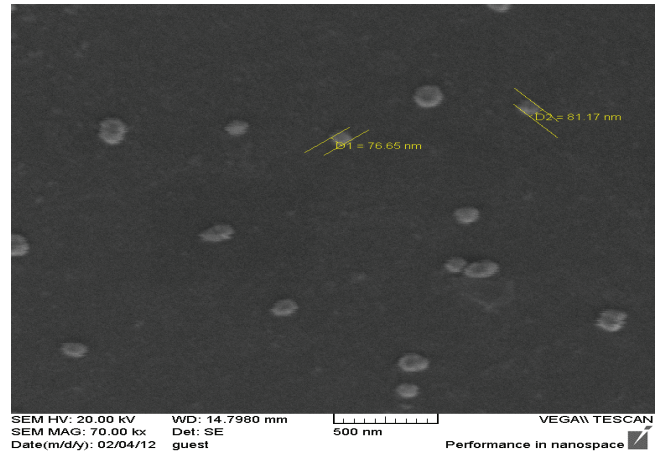


Fig. 6. SEM image of nano-Fe<sub>3</sub>O<sub>4</sub>.

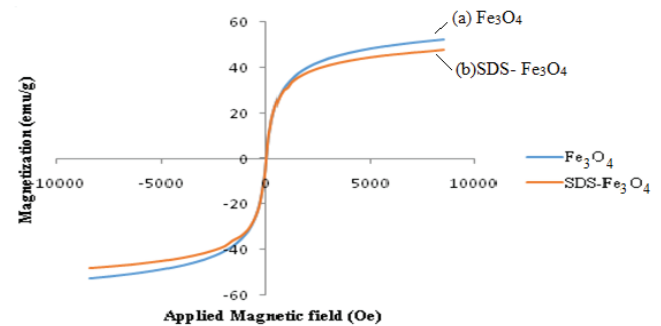


Fig. 7. VSM magnetization curves of nano-Fe<sub>3</sub>O<sub>4</sub> (a) and nano-Fe<sub>3</sub>O<sub>4</sub>-SDS (b).

magnet. However, all evidences such as FT-IR spectrum, XRD, SEM and the VSM analysis confirmed the formation of phase of iron oxide nano-particles.

### 3.2.3. TGA analysis

To estimate the amount of surfactant deposited onto the surface of nano-Fe<sub>3</sub>O<sub>4</sub>, the TGA of nano-Fe<sub>3</sub>O<sub>4</sub> and nano-Fe<sub>3</sub>O<sub>4</sub>-SDS was conducted, and the result is shown in Fig. 8. Upon heating in TGA, the nano-Fe<sub>3</sub>O<sub>4</sub>-SDS losses weight about 1.0% at temperatures ranging from 70°C to 120°C, mainly due to the loss of physically adsorbed water on the material. The weight loss of nano-Fe<sub>3</sub>O<sub>4</sub>-SDS occurred in the temperature range of 200°C–400°C was due to the decomposition of SDS. At temperatures above 500°C the SDS was completely decomposed, and the residual weight should be the lonely the weight of Fe<sub>3</sub>O<sub>4</sub>. According to the TGA curves, the SDS content of nano-Fe<sub>3</sub>O<sub>4</sub>-SDS was evaluated to be 20.3% by weight [19,28,40,42]. However all these evidences confirm that the nano-Fe<sub>3</sub>O<sub>4</sub> is coated well with SDS and hemimicelles of nano-Fe<sub>3</sub>O<sub>4</sub>-SDS was formed.

## 3.3. Multivariate optimization strategy

### 3.3.1. Modelling via a Box–Behnken design approach

In this study the BBD methodology was used to determine the effects of the main operating variables on BG adsorption and to find the combination of variables resulting

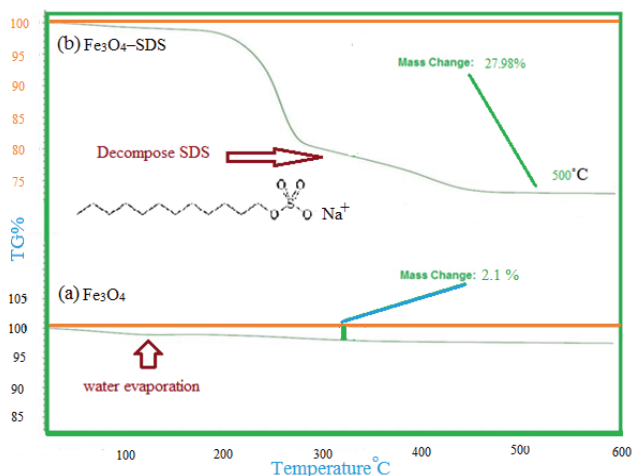


Fig. 8. TGA curves of both nano-Fe<sub>3</sub>O<sub>4</sub> (a) and nano-Fe<sub>3</sub>O<sub>4</sub>-SDS (b).

in maximum adsorption efficiency. Four independent variables, namely the nano-Fe<sub>3</sub>O<sub>4</sub> dose (*N*) and surfactant amount (*S*), initial dye concentration (*C<sub>d</sub>*) and initial solution pH, were chosen as the critical variables and are shown in Table 1. A 27-run BBD with four factors at three levels, including three replicates at the centre point ( $N = 4 \times 2 \times 3 + 3$ ), was used for finding a second-order response surface model. The three centre point runs were added to provide as a measure of process stability and inherent variability (Table 2) [35–38]. By applying multiple regression analysis on the design matrix (Table 2), the following second-order polynomial equation was established and estimated effects and coefficients for the suggested second-order models (Tables 3 and 4) have been obtained to illuminate both the BG removal percent (*R*%) and absorption capacity (*q*) by nano-Fe<sub>3</sub>O<sub>4</sub>-SDS:

$$\begin{aligned} \%R = & 60.13 + 14.225 S + 13.603 N - 9.958 \text{ pH} - 18.530 C_d \\ & - 2.318 S \times S - 6.151 N \times N - 4.443 \text{ pH} \times \text{pH} \\ & + 2.474 C_d \times C_d - 4.25 S \times N - 7.38 S \times \text{pH} - 2.25 S \\ & \times C_d - 2.50 N \times \text{pH} - 2.94 N \times C_d \end{aligned} \quad (4)$$

$$\begin{aligned} q = & 300.67 - 23.25 S - 85.44 N - 48.05 \text{ pH} + 121.83 C_d \\ & + 12.49 N \times N - 24.08 \text{ pH} \times \text{pH} - 55.85 C_d \\ & \times C_d + 24.32 S \times N - 23.26 S \times \text{pH} - 6.30 S \times C_d \\ & + 16.22 N \times \text{pH} - 32.64 N \times C_d + 27.86 \text{ pH} \times C_d \end{aligned} \quad (5)$$

where *q* is the uptake capacity; *R*%: removal percent of BG, *S*: SDS, *N*: nano-Fe<sub>3</sub>O<sub>4</sub>, *C<sub>d</sub>*: dye concentration.

The significance of the coefficients model, the independent variables and their interactions were tested and are shown in Table 5. Analysis of variances (ANOVA) was used to check the adequacy and validity of the suggested models. As seen in Table 5, the ANOVA results of the regression models (Eqs. (4) and (5)) showed that the quadratic model was highly significant, which was an evident from the Fisher's *F*-test. The larger *F* values of (152.67 and 155.03, for *R*% and *q*, respectively) and smaller *p* values (<0.05) indicate that the model terms are significant [25,26,38]. The “lack-of-fit” *p* values imply that it is not significant compared with experimental pure error. Besides of ANOVA, model adequacy was also checked by obtaining the coefficient of determination *R*<sup>2</sup>, the adjusted coefficient of determination *R*<sup>2</sup><sub>adj</sub> and an analysis of residuals [35–38].

Table 3  
Estimated effects and regression coefficients and statistical parameters of the suggested model for *R*%

| Term  | Effect  | Coefficient | SE          | <i>T</i> | <i>p</i> |
|---|---------|-------------|-------------|----------|----------|
|   |         |             | coefficient | value    | Value    |
| Constant                                    |         | 60.13       | 1.29        | 46.45    | 0.000    |
| <i>S</i>                                    | 28.450  | 14.225      | 0.647       | 21.97    | 0.000    |
| <i>N</i>                                    | 27.206  | 13.603      | 0.647       | 21.01    | 0.000    |
| pH  | -19.917 | -9.958      | 0.647       | -15.38   | 0.000    |
| <i>C<sub>d</sub></i>                        | -37.060 | -18.530     | 0.647       | -28.62   | 0.000    |
| <i>S</i> × <i>S</i>                         | -4.637  | -2.318      | 0.971       | -2.39    | 0.034    |
| <i>N</i> × <i>N</i>                         | -12.301 | -6.151      | 0.971       | -6.33    | 0.000    |
| pH × pH                                     | -8.887  | -4.443      | 0.971       | -4.58    | 0.001    |
| <i>C<sub>d</sub></i> × <i>C<sub>d</sub></i> | 4.949   | 2.474       | 0.971       | 2.55     | 0.026    |
| <i>S</i> × <i>N</i>                         | -8.50   | -4.25       | 1.12        | -3.79    | 0.003    |
| <i>S</i> × pH                               | -14.75  | -7.38       | 1.12        | -6.58    | 0.000    |
| <i>S</i> × <i>C<sub>d</sub></i>             | -4.50   | -2.25       | 1.12        | -2.01    | 0.068    |
| <i>N</i> × pH                               | -5.00   | -2.50       | 1.12        | -2.23    | 0.046    |
| <i>N</i> × <i>C<sub>d</sub></i>             | -5.88   | -2.94       | 1.12        | -2.62    | 0.022    |

Note: SE – standard error.

Table 4  
Estimated effects and regression coefficients and statistical parameters of the suggested model for *q*

| Term  | Effect  | Coefficient | SE          | <i>T</i> | <i>p</i> |
|---|---------|-------------|-------------|----------|----------|
|   |         |             | coefficient | value    | Value    |
| Constant                                    |         | 300.67      | 7.20        | 41.74    | 0.000    |
| <i>S</i>                                    | -46.50  | -23.25      | 3.60        | -6.46    | 0.000    |
| <i>N</i>                                    | -170.88 | -85.44      | 3.60        | -23.72   | 0.000    |
| pH  | -96.10  | -48.05      | 3.60        | -13.34   | 0.000    |
| <i>C<sub>d</sub></i>                        | 243.66  | 121.83      | 3.60        | 33.83    | 0.000    |
| <i>N</i> × <i>N</i>                         | 24.99   | 12.49       | 5.40        | 2.31     | 0.039    |
| pH × pH                                     | -48.16  | -24.08      | 5.40        | -4.46    | 0.001    |
| <i>C<sub>d</sub></i> × <i>C<sub>d</sub></i> | -111.70 | -55.85      | 5.40        | -10.34   | 0.000    |
| <i>S</i> × <i>N</i>                         | 48.63   | 24.32       | 6.24        | 3.90     | 0.002    |
| <i>S</i> × pH                               | -46.52  | -23.26      | 6.24        | -3.73    | 0.003    |
| <i>S</i> × <i>C<sub>d</sub></i>             | -12.59  | -6.30       | 6.24        | -1.01    | 0.333    |
| <i>N</i> × pH                               | 32.44   | 16.22       | 6.24        | 2.60     | 0.023    |
| <i>N</i> × <i>C<sub>d</sub></i>             | -65.27  | -32.64      | 6.24        | -5.23    | 0.000    |
| pH × <i>C<sub>d</sub></i>                   | -55.71  | -27.86      | 6.24        | -4.47    | 0.001    |

Note: SE – standard error.

A higher value of *R*<sup>2</sup> is desirable, as it is interpreted as the percent of variability in the response explained by the proposed models. The obtained values of *R*<sup>2</sup> and *R*<sup>2</sup><sub>adj</sub> for the earlier mentioned models (for *R*%; *R*<sup>2</sup> = 99.44%; *R*<sup>2</sup><sub>adj</sub> = 98.79%; for *q*: *R*<sup>2</sup> = 99.45%; *R*<sup>2</sup><sub>adj</sub> = 98.81%) are satisfactory. Furthermore, the model adequacy was also investigated by assessment of the residuals ( $e = R_{exp} - R_{pred}$ ). The residual analysis outlines a good concordance between experimental (*R*<sub>exp</sub>) and predicted (*R*<sub>pred</sub>) responses. Further, the normal probability plot shows that the distribution of residuals is normal and the model satisfies the assumptions of the ANOVA (figures not shown) [4,17,25,26]. The response surfaces plots clearly represent the effect of experimental variables and their mutual interactions

Table 5  
Analysis of variance (ANOVA) for both suggested model for adsorption responses  $R\%$  and  $q$

| Source         | DF | Seq SS   | Adj SS   | Adj MS   | F value | p Value |
|----------------|----|----------|----------|----------|---------|---------|
| <i>R%</i>      |    |          |          |          |         |         |
| Regression     | 14 | 10,748.2 | 10,748.2 | 767.73   | 152.67  | 0.000   |
| Linear         | 4  | 9,959.0  | 9,959.0  | 2,489.76 | 495.12  | 0.000   |
| Square         | 4  | 407.3    | 407.3    | 101.83   | 20.25   | 0.000   |
| Interaction    | 6  | 381.9    | 381.9    | 63.65    | 12.66   | 0.000   |
| Residual error | 12 | 60.3     | 60.3     | 5.03     |         |         |
| Lack-of-fit    | 10 | 59.5     | 59.5     | 5.95     | 14.76   | 0.065   |
| Pure error     | 2  | 0.8      | 0.8      | 0.40     |         |         |
| Total $R\%$    | 26 | 10,808.6 |          |          |         |         |
| <i>q</i>       |    |          |          |          |         |         |
| Regression     | 14 | 337,846  | 337,846  | 24,132   | 155.03  | 0.000   |
| Linear         | 4  | 299,906  | 299,906  | 74,977   | 481.66  | 0.000   |
| Square         | 4  | 24,835   | 24,835   | 6,209    | 39.89   | 0.000   |
| Interaction    | 6  | 13,105   | 13,105   | 2,184    | 14.03   | 0.000   |
| Residual error | 12 | 1,868    | 1,868    | 156      |         |         |
| Lack-of-fit    | 10 | 1,848    | 1,848    | 185      | 18.33   | 0.053   |
| Pure error     | 2  | 20       | 20       | 10       |         |         |
| Total ( $q$ )  | 26 | 339,714  |          |          |         |         |

Note: For  $R\%$ :  $R^2 = 99.44\%$ ;  $R^2_{adj} = 98.79\%$ ;  $R^2_{pred} = 96.81\%$ .

For  $q$ :  $R^2 = 99.45\%$ ;  $R^2_{adj} = 98.81\%$ ;  $R^2_{pred} = 96.85\%$ .

DF – degrees of freedom; Seq SS – sum of squares; Adj SS – adjusted sum squares; Adj MS – adjusted mean square;  $F$  – Fischer ratio; and  $p$  value – significance level.

on responses. As can be observed from Fig. 9, the predicted model for  $q$  is visualized by the equation of responses as a function of two independent variables, while the third one is kept constant (at the middle point).

### 3.3.2. Simultaneous optimization of $R\%$ and $q$ using desirability function

In the adsorption process two aspects were evident: the removal percent ( $R\%$ ) and uptake capacity ( $q$ ) was obtained; and simultaneous optimization was more favourable from both environmental and economic viewpoints [38]. This is due to the more favourable results for the highest removal percent, with the least amount of adsorbent usage [38]. The high removal efficiency ensures that the adequate removal of dye and high uptake capacity leads to a lower usage of adsorbent and avoids excess waste production. Using Derringer's desirability function for simultaneous optimization of obtained responses is a conventional and straightforward method [4,35,38,43]. In this approach, the global response, derived through Derringer's desirability function, is to first convert the response into an individual desirability function ( $d_i$ ) that varies from 0 to 1 (lowest to highest desirability) and then combine these into overall desirability function,  $D$ , by computing their geometric mean of different  $d_i$  values would reach 1 as maximum value [4,35,38,43]:

$$D = \sqrt[m]{d_1 d_2 \dots d_m} \quad (6)$$

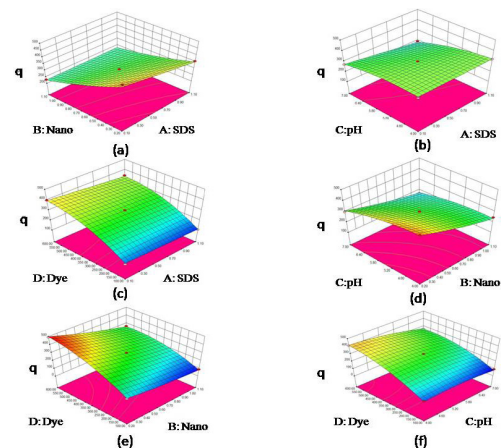


Fig. 9. Response surface plots showing effective factors and their mutual effects on uptake capacity ( $q$ ) of BG dye while the other variables are at center level: (a) the effect of SDS amount and nano amount; (b) the effect of SDS amount and pH; (c) the effect of initial BG dye concentration and SDS amount; (d) the effect of nano amount and pH; (e) the effect of nano amount and initial BG dye concentration; and (f) the effect of pH and initial BG dye concentration.

where  $d_i$  indicates the desirability of the response, and  $m$  is the number of responses in the measure. Running the statistical software of MINITAB17 enables simultaneous optimization of multiple responses to be attained. These results for simultaneous optimization are:  $R\% = 62$  and  $q = 440$  mg/g

with overall desirability 0.99 in  $C_d = 600$  mg/L, pH = 4, nano- $\text{Fe}_3\text{O}_4 = 8.8$  mg and SDS = 10.1 mg. While individual optimization takes place for a maximum of  $R\% = 88$  at  $C_d = 376.6$  mg/L, pH = 4, nano- $\text{Fe}_3\text{O}_4 = 10.9$  mg and SDS = 11.8 mg and a maximum  $q = 460$  mg/g at  $C_d = 600$  mg/L, pH = 4, nano- $\text{Fe}_3\text{O}_4 = 8.2$  mg and SDS = 6 mg.

### 3.4. Solid-phase extraction

#### 3.4.1. Pre-concentration procedure and regeneration studies

The nano- $\text{Fe}_3\text{O}_4$ -SDS as mixed hemimicelles proposed and applied for pre-concentration of BG in environmental water samples through a SPE method [6,16,22,23,30–33]. Under optimized conditions the pre-concentration process was carried out. The nano- $\text{Fe}_3\text{O}_4$ -SDS adsorbent was prepared through the addition of 8.83 g nano- $\text{Fe}_3\text{O}_4$  with 10.8 g SDS in 250 mL filtered water; its pH was adjusted to about 4.0 with 0.1 M HCl containing 5–300  $\mu\text{g/L}$  BG. Then the sample solution was stirred by a mechanical mixture. By the rapid isolating of nano- $\text{Fe}_3\text{O}_4$ -SDS through placing a strong magnet on the bottom of beaker, after 5 min the solution became clear and was decanted.

To evaluate the possibility of regeneration and reusability of the nano- $\text{Fe}_3\text{O}_4$ -SDS, desorption experiments were performed as following. A 2.5 mL acetic acid as a desorbed solvent was added to enriched nano- $\text{Fe}_3\text{O}_4$ -SDS with BG (nano- $\text{Fe}_3\text{O}_4$ -SDS-BG) in a beaker. The beaker was placed on the magnet, and the mixture was decanted again. The absorption of the solution separated from nano- $\text{Fe}_3\text{O}_4$  magnetically and was measured spectrophotometrically at 629 nm. Desorption procedures were carried out with a quantitative recovery above 95% of BG. The regeneration investigation was also performed according to the abovementioned manner, and it is found that adsorption capacity ( $q_{\text{max}}$ ) and enrichment factor diminish from 480 to 390 mg/L and 63 to 48, respectively.

It can be pointed out that previously desorption of BG from the nano- $\text{Fe}_3\text{O}_4$ -SDS was examined with different organic solvents (acetonitrile, methanol, acetone, ethyl acetate, ethanol, acetic acid) and acetic acid was the best choice as the desorption solvent [6,16,22,23,30–33].

#### 3.4.2. Interference studies

In this study, separation, determination and the tolerance limit of BG were carried out in the presence of coexisting ions and dyes, causing a change in maximum acceptable absorbance of less than  $\pm 5\%$ . Under optimum experimental conditions, matrix effects due to the presence of some foreign ions and two dyes (toluidine blue, basic blue) on the determination and adsorption process of BG by the nano- $\text{Fe}_3\text{O}_4$ -SDS were examined. For this purpose, a aliquot solution containing 10.0 mg/L BG and 0.02 g nano- $\text{Fe}_3\text{O}_4$  along with 0.01 g SDS was examined (at pH 4.0), and the results are shown in Table 6. The table shows that toluidine blue and basic blue are extremely interfered even at the same concentration as that of BG, whereas most of the investigated species did not interfere during the separation, elimination and determination.

Table 6  
Effect of coexisting ions on adsorption of BG onto nano- $\text{Fe}_3\text{O}_4$ -SDS

| Foreign ion  | Tolerance limit (mg/L) |
|--|------------------------|
| $\text{Ag}^+$ , $\text{Na}^+$ , $\text{NO}_3^-$ , $\text{Cl}^-$ , $\text{F}^-$ , $\text{Mg}^{2+}$ , $\text{Zn}^{2+}$ , $\text{Cu}^{2+}$ , $\text{Ni}^{2+}$ | 600                    |
| $\text{K}^+$ , $\text{Al}^{3+}$  | 400                    |
| $\text{CO}_3^{2-}$   | 100                    |
| Toluidine blue and basic blue  | 10                     |

<sup>a</sup>All cations were prepared from nitrate salts, and anions were prepared from sodium and potassium salts.

#### 3.4.3. Analytical parameters

The calibration curve was found through a regression model as  $y = 0.272 + 7.924x$  ( $y$ : absorbance;  $x$ : dye concentration ( $\mu\text{g/L}$ )), with a linear range from 5 to 400  $\mu\text{g/L}$ , and coefficient of determination  $R^2 = 0.9999$ . Relative standard deviation for 21.4  $\mu\text{g/L}$  was 2.1% ( $n = 9$ ), and the limit of detection was 3.0  $\mu\text{g/L}$  ( $S/N = 3$ ). The enrichment factor of the pre-concentration method was estimated from ratio of slopes of calibration curves with (7.924) and without a pre-concentration steps (0.125) and found to be 63 [44].

### 3.5. Adsorption isotherms

The adsorption isotherms, through a description of adsorbate and adsorbent behaviour, provide a quantitative estimation of adsorption capacity or maximum removal capacity of pollutant per unit mass of sorbent. In this study, the Langmuir, Freundlich, Dubinin–Radushkevich (D–R) sorption isotherms were investigated [45–53]. Through this, both linear and non-linear curve analysis of various isotherms were examined. Following this, statistical error analysis was used as a significance criterion for non-linear fitting of the isotherms to the equilibrium experimental data. Thus, the coefficient of determination ( $R^2$ ), normalized standard deviation ( $\Delta q$ ), and Chi-square ( $\chi^2$ ) statistics were calculated as follows [7,18,26,47–49]:

$$R^2 = \frac{\sum (q_{e,\text{exp}} - q_{e,\text{cal}})^2}{\sum [(q_{e,\text{exp}} - q_{e,\text{cal}})^2 + (q_{e,\text{exp}} - q_{e,\text{cal}})^2]} \quad (7)$$

$$\Delta q = \sqrt{\frac{\sum [(q_{e,\text{exp}} - q_{e,\text{cal}}) / q_{e,\text{exp}}]^2}{n - 1}} \quad (8)$$

$$\chi^2 = \sum \frac{(q_{e,\text{exp}} - q_{e,\text{cal}})^2}{q_{e,\text{cal}}} \quad (9)$$

where  $n$  is the number of data points;  $q_{e,\text{exp}}$  is the equilibrium adsorption uptake capacity from the experiment (mg/g); and  $q_{e,\text{cal}}$  is the equilibrium capacity calculated according to the dynamic model (mg/g). A small value of  $\chi^2$  indicates that data from the model is similar to the experimental value [18,47,49]. The Langmuir isotherm is investigated first, assuming that the adsorbate is removed from the aqueous phase on the homogeneous surface by monolayer sorption without interactions between sorbate molecules, and the

adsorption of each dye molecule onto the surface has equal adsorption activation energy. Graphically, a plateau characterizes the Langmuir isotherm. Therefore, at equilibrium, a saturation point is reached where no further adsorption can occur (Fig. 10). Once a dye molecule occupies a site, no further adsorption can take place at that site [41,43–47], while the Freundlich isotherm is an empirical equation proving that the adsorption process takes place on heterogeneous surfaces with a non-uniform distribution for heat of adsorption over the surface, and a multilayer adsorption can be expressed [45–53].

The non-linear and linear isotherms of Langmuir and Freundlich are represented by the following equations (Eqs. (10)–(13)), respectively:

$$q_e = \frac{q_{\max} b C_e}{1 + b C_e} \quad (10)$$

$$\frac{C_e}{q_e} = \frac{1}{b q_{\max}} + \frac{C_e}{q_{\max}} \quad (11)$$

$$q_e = K_f C_e^{1/n} \quad (12)$$

$$\ln q_e = \frac{1}{n} \ln C_e + \ln K_f \quad (13)$$

where  $q_{\max}$  is the maximum adsorption capacity (mg/g);  $q_e$  is the adsorption capacity at equilibrium (mg/g);  $b$  is the Langmuir isotherm constant (L/mg) that indicates site energy factor, representing adsorption affinity. The higher  $b$  is the higher the affinity of the sorbent for the sorbate;  $C_e$  is the equilibrium concentration of sorbate in the solution (mg/L);  $K_f$  is the Freundlich isotherm constant ((mg/g)(L/mg)<sup>1/n</sup>); and  $1/n$  is adsorption intensity.  $1/n$  values indicate the type of isotherm to be irreversible when  $1/n$  equals 0, favourable ( $0 < 1/n < 1$ ), or unfavourable ( $1/n > 1$ ) [43,45–49,52,53]. The maximum monolayer adsorption of BG onto nano-Fe<sub>3</sub>O<sub>4</sub>-SDS was found to be 480 mg/g; adsorption affinity  $b$  was equal to 0.13 L/mg; and the Freundlich constant was obtained

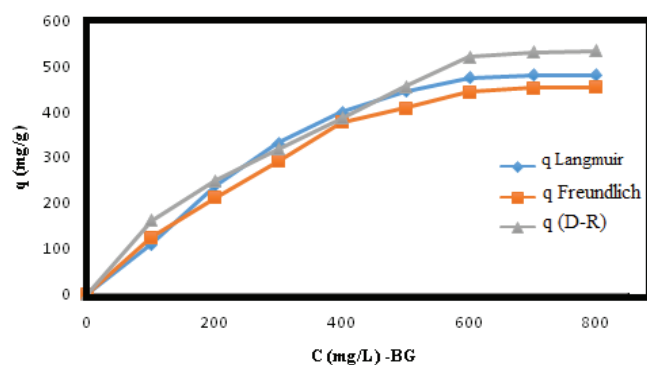


Fig. 10. Non-linear Isotherms Langmuir, Freundlich, and Dubinin–Radushkevich model considered for removal of Brilliant Green by nano-Fe<sub>3</sub>O<sub>4</sub>-SDS.

as 28.5 mg/g. The  $1/n$  obtained was equal to 0.51, which means the dye adsorption is chemically favourable [45,46]. The experimental equilibrium data is better fitted to both linear Langmuir ( $R^2 = 0.9927$ ) and Freundlich ( $R^2 = 0.9926$ ), but non-linear isotherm fitting shows the better criteria for Freundlich ( $R^2 = 0.990$ ,  $\chi^2 = 12.6$ ,  $\Delta q = 2.38$ ) than Langmuir ( $R^2 = 0.988$ ;  $\chi^2 = 26.25$ ;  $\Delta q = 5.26$ ), and overall, it is depicted that the monolayer adsorption is the predominant manner of dye coverage on the adsorbent [18,47,48].

Further information about the adsorption behaviour of BG was also examined with D–R isotherm model, which is more general than Langmuir. The D–R model is often applied to estimate the characteristic porosity and apparent free energy of adsorption. The D–R equation is generally expressed as follows [43,45–49]:

$$q_e = q_{\max} \exp(-B(RT \ln[1 + \frac{1}{C_e}])^2) \quad (14)$$

where  $B$  is a constant related to the adsorption energy;  $R$  (8.314 J/mol K) is the gas constant; and  $T$  (K) is the absolute temperature. The constant  $B$  (mol<sup>2</sup>/kJ<sup>2</sup>) gives the mean free energy  $E$  (kJ/mol) of sorption per molecule of the sorbate (BG) when it is transferred to the surface of the solid (nano-Fe<sub>3</sub>O<sub>4</sub>-SDS) from infinity in the solution, and can be calculated using the following relationship:

$$E = 1 / (2\beta)^{1/2} \quad (15)$$

This parameter ( $E$ ) imparts information about chemical or physical adsorption. If the magnitude of  $E$  lies between 8 and 16 kJ/mol, the adsorption process follows chemical ion exchange, while for the values of  $E < 8$  kJ/mol the adsorption process turns to a physical nature [43,45–49]. The mean free energy of BG adsorption was found to be 12.8 kJ/mol, which indicates that the adsorption process of BG onto nano-Fe<sub>3</sub>O<sub>4</sub>-SDS may occur via a chemical interaction. This is confirmed by the  $n$  value obtained from the Freundlich isotherm (0.51), which implies that chemisorption has taken place [45,46].

However, the linear Langmuir model exhibits the best fitting to the experimental data, which may be deduced from its highest  $R^2$  (0.9927) (Table 7). Therefore, the adsorption of BG on nano-Fe<sub>3</sub>O<sub>4</sub>-SDS can happen by homogeneous and monolayer, with a significant value for uptake capacity of 471 mg/g.

### 3.6. Thermodynamic parameters

It is well known that the temperature in the adsorption process has a crucial effect on the adsorption of sorbate. The thermodynamic parameters calculated using Gibbs free energy change are related to the equilibrium constant by using the following equations [7,44–47]:

$$\Delta G^\circ = -RT \ln K \quad (16)$$

where  $K$  is the equilibrium constant [48,49].

Table 7  
Constant parameters and different criteria calculated for both linear non-linear fitting of various adsorption isotherms

| Isotherm model | Parameters                           |  |        | Errors   | Criteria   |
|----------------|--------------------------------------|--|--------|----------|------------|
| Langmuir       | $q_{\max}$ (mg/g)                    | $B$ (L/mg)                               | $R^2$  | $\chi^2$ | $\Delta q$ |
| Non-linear     | 471                                  | 0.11                                     | 0.988  | 26.25    | 5.26       |
| Linear         | 480                                  | 0.13                                     | 0.9927 |          |            |
| Freundlich     | $K_f$ ((mg/g)(L/mg) <sup>1/n</sup> ) | $1/n$                                    |        |          |            |
| Non-linear     | 36.59                                | 0.482                                    | 0.990  | 12.67    | 2.38       |
| Linear         | 28.5                                 | 0.51                                     | 0.9926 |          |            |
| D–R            | $q_{\max}$ (mg/g)                    | $B$ (mol <sup>2</sup> /kJ <sup>2</sup> ) |        |          |            |
| Non-linear     | 221.37                               | 0.003                                    | 0.966  | 110.81   | 35.12      |
| Linear         | 344.21                               | 0.002                                    | 0.76   |          |            |

$$K = \frac{C_b}{C_a} \quad (17)$$

where  $C_a$  and  $C_b$  are the equilibrium concentration of BG in the solution and on the sorbent. According to thermodynamics, the  $\Delta G^\circ$  change is also related to entropy change, and heat of adsorption at constant temperature and wide range of temperature variation causes a change in thermodynamic parameters that could be estimated by the following equation [7,17,18,46–53].

$$\Delta G^\circ = \Delta H^\circ - T \Delta S^\circ \quad (18)$$

$$\ln K = \frac{-\Delta G^\circ}{RT} = \frac{\Delta S^\circ}{R} - \frac{\Delta H^\circ}{RT} \quad (19)$$

where  $\Delta G^\circ$  is the Gibbs free energy change (J/mol);  $\Delta H^\circ$  the change in enthalpy (J/mol);  $\Delta S^\circ$  the entropy change (J/mol K);  $T$  the absolute temperature (K); and  $R$  the universal gas constant (8.314 J/mol K). The  $\Delta H^\circ$  and  $\Delta S^\circ$  could be determined by the slope and intercept of the linear van't Hoff plot, i.e., as  $\ln K$  vs.  $(1/T)$  (figure not shown).  $\Delta H^\circ = 16.2$  kJ/mol and  $\Delta S^\circ = 48.9$  J/mol K are found, due to changes of  $\Delta G^\circ$  from 20°C to 50°C.  $\Delta G^\circ$  is equal to 1.8 kJ/mol at 20°C. The positive Gibbs energy values indicate the non-spontaneous nature of the adsorption process, and  $\Delta H^\circ > 0$  shows that the process is endothermic. A positive  $\Delta S^\circ$  value indicated an increase in the degrees of freedom of the adsorbed species, and the positive value of  $\Delta S^\circ$  suggests an accidental increase at the solid/solution interface, with structural changes in the BG and adsorbent [7,18,19,25,26,45–53].

However, according to the results obtained in this study, the chemisorption has a predominant portion on the adsorption mechanism. This observation can be justified with the following argument: FT-IR spectra analysis shows that functional groups of nano-Fe<sub>3</sub>O<sub>4</sub>-SDS involved in adsorption, along with better fitting experimental data to the linear Langmuir isotherm ( $R^2 = 0.9927$ ); it can be an indication of the chemical coverage of sorbent, accompanied by a better description by D–R isotherms results [45,46].

As a final point, comparison of the adsorption capacity of BG by other adsorbents is shown in Table 8. These results showed that the nano-Fe<sub>3</sub>O<sub>4</sub>-SDS has an excellent potential (480 mg/g) for the removal of dyes from an aqueous solution [6,7,25,54–58].

Table 8  
Adsorption capacity ( $q_{\max}$ ) of Brilliant Green with some different adsorbents

| Adsorbent  | $q_{\max}$ (mg/g) | Reference  |
|--|-------------------|------------|
| Zinc oxide nano-particles                          | 142               | [6]        |
| Rice husk ash                                      | 26                | [7]        |
| SDS-modified alumina                               | 168               | [25]       |
| Kaolin   | 65                | [54]       |
| NaOH-treated saw dust                              | 58                | [55]       |
| Red clay   | 125               | [56]       |
| Bagasse fly ash                                    | 133.3             | [57]       |
| Diatomite-attapulgite composite                    | 100               | [58]       |
| Nano-size nano-Fe <sub>3</sub> O <sub>4</sub> -SDS | 480               | This study |

#### 4. Conclusion

The nano-Fe<sub>3</sub>O<sub>4</sub>-SDS is introduced as a novel and efficient adsorbent for removal and SPE of BG from aqueous solutions. The effective factors, e.g., pH, sorbent dosage ( $m$ ) and initial concentration of BG ( $C_a$ ) were considered in terms of removal efficiency ( $R\%$ ) and uptake capacity ( $q$ ). RSM involving BBD was employed to optimize the relationship between effective factors and responses. According to the results, using Derringer's function, the simultaneous optimization of both responses was reported, and the values were obtained as  $R\% = 62\%$  and  $q = 440$  mg/g, with an overall desirability of 0.99 in  $C_a = 600$  mg/L, pH = 4, nano-Fe<sub>3</sub>O<sub>4</sub> = 8.8 mg and SDS = 10.1 mg. The Langmuir isotherm model matched better with the equilibrium data than others, with a maximum monolayer of BG 480 mg/g. The thermodynamic evaluation of the current adsorption system revealed that the adsorption procedure is spontaneous and endothermic in its nature. It is used as an efficient solid-phase extractor of BG from aqueous water with a significance enrichment factor of about 63. The morphology and properties of the produced magnetite nano-particles was determined by SEM, XRD, VSM, FT-IR and TGA. All results show that chemisorption is likely to be a predominant portion of the adsorption process. Based on the entire conclusion, nano-Fe<sub>3</sub>O<sub>4</sub>-SDS shows high potential to be used for removal of BG from aqueous mediums.

## References

- [1] E. Forgacs, T. Cserháti, G. Oros, Removal of synthetic dyes from wastewaters: a review, *Environ. Int.*, 30 (2004) 953–971.
- [2] G. Crini, Non-conventional low-cost adsorbents for dye removal: a review, *Bioresour. Technol.*, 97 (2006) 1061–1085.
- [3] V.G. Gupta, Suhas, Application of low-cost adsorbents for dye removal – a review, *J. Environ. Manage.*, 90 (2009) 2013–2042.
- [4] J. Zolgharnein, Z. Adhami, A. Shahmoradi, S.N. Mousavi, Optimization of removal of methylene blue by *Platanus* tree leaves using response surface methodology, *Anal. Sci.*, 26 (2010) 111–116.
- [5] K.G. Bhattacharyya, A. Sarma, Adsorption characteristics of the dye, Brilliant Green, on Neem leaf powder, *Dyes Pigm.*, 57 (2003) 211–222.
- [6] M. Ghaedi, G. Negintaji, H. Karimi, F. Marahel, Solid phase extraction and removal of brilliant green dye on zinc oxide nanoparticles loaded on activated carbon: new kinetic model and thermodynamic evaluation, *J. Ind. Eng. Chem.*, 20 (2014) 1444–1452.
- [7] V.S. Mane, I.D. Mall, V.C. Srivastav, Kinetic and equilibrium isotherm studies for the adsorptive removal of Brilliant Green dye from aqueous solution by rice husk ash, *J. Environ. Manage.*, 84 (2007) 390–400.
- [8] C. Fernandez, M.S. Larrechi, M.P. Callao, An analytical overview of processes for removing organic dyes from wastewater effluents, *TrAC Trends Anal. Chem.*, 29 (2010) 1202–1211.
- [9] J. Zolgharnein, A. Shahmoradi, J. Ghasemi, Pesticides removal using conventional and low-cost adsorbents: a review, *Clean*, 39 (2011) 105–119.
- [10] P. Xu, G.M. Zeng, D.L. Huang, C.L. Feng, S. Hu, M.H. Zhao, C. Lai, Z. Wei, C. Huang, G.X. Xie, Z.F. Liu, Use of iron oxide nanomaterials in wastewater treatment: a review, *Sci. Total Environ.*, 424 (2012) 1–10.
- [11] M. Hua, S. Zhang, B. Pan, W. Zhang, L. Lv, Q. Zhang, Heavy metal removal from water/wastewater by nanosized metal oxides: a review, *J. Hazard. Mater.*, 211–212 (2012) 317–331.
- [12] M. Khajeh, S. Laurent, K. Dastafkan, Nano-adsorbents: classification, preparation, and applications (with emphasis on aqueous media), *Chem. Rev.*, 113 (2013) 7728–7768.
- [13] Y.F. Shen, J. Tang, Z.H. Nie, Y.D. Wang, Y. Ren, L. Zuo, Preparation and application of magnetic  $\text{Fe}_3\text{O}_4$  nanoparticles for wastewater purification, *Sep. Purif. Technol.*, 68 (2009) 312–319.
- [14] S. Mak, D. Chen, Fast adsorption of methylene blue on polyacrylic acid-bound iron oxide, *Dyes Pigm.*, 61 (2004) 93–98.
- [15] M. Mahdavi, M.B. Ahmad, M.J. Haron, F. Namvar, B. Nadi, M.Z. Ab Rahman, J. Amin, Synthesis, surface modification and characterisation of biocompatible magnetic iron oxide nanoparticles for biomedical applications, *Molecules*, 18 (2013) 7533–7548.
- [16] X. Zhao, Y. Shi, Y. Cai, S. Mou, Cetyltrimethyl ammonium bromide-coated magnetic nanoparticles for the preconcentration of phenolic compounds from environmental water samples, *Environ. Sci. Technol.*, 42 (2008) 1201–1206.
- [17] J. Zolgharnein, Z. Choghaei, M. Bagtash, Sh. Feshki, M. Rastgordani, P. Zolgharnein, Nano- $\text{Fe}_3\text{O}_4$  and corn cover composite for removal of Alizarin Red S from aqueous solution: characterization and optimization investigations, *Desal. Wat. Treat.*, 57 (2016) 27672–27685.
- [18] R.K. Gautam, V. Rawat, S. Banerjee, M.A. Sanroman, S. Soni, S.K. Singh, M.C. Chattopadhyaya, Synthesis of bimetallic Fe–Zn nanoparticles and its application towards adsorptive removal of carcinogenic dye malachite green and Congo red in water, *J. Mol. Liq.*, 212 (2015) 227–236.
- [19] R.K. Gautam, P.K. Gautam, S. Banerjee, S. Soni, S.K. Singh, M.C. Chattopadhyaya, Removal of Ni(II) by magnetic nanoparticles, *J. Mol. Liq.*, 204 (2015) 60–69.
- [20] G. Giakissikli, A.N. Anthemidis, Magnetic materials as sorbents for metal/metalloid preconcentration and/or separation. A review, *Anal. Chim. Acta*, 789 (2013) 1–16.
- [21] K. Aguilar-Arteaga, J.A. Rodriguez, E. Barrado, Magnetic solids in analytical chemistry, *Anal. Chim. Acta*, 674 (2010) 157–165.
- [22] B. Zargar, H. Parham, A. Hatamie, Modified iron oxide nanoparticles as solid phase extractor for spectrophotometric determination and separation of basic fuchsin, *Talanta*, 77 (2009) 1328–1331.
- [23] A. Afkhami, R. Moosavi, T. Madrakian, Preconcentration and spectrophotometric determination of low concentrations of malachite green and leuco-malachite green in water samples by high performance solid phase extraction using maghemite nanoparticles, *Talanta*, 82 (2010) 785–789.
- [24] M. Bagtash, Y. Yamini, E. Tahmasebi, J. Zolgharnein, Z. Dalirnasab, Magnetite nano-particles coated with tannic acid as a viable sorbent for solid-phase extraction of  $\text{Cd}^{2+}$ ,  $\text{Co}^{2+}$  and  $\text{Cr}^{3+}$ , *Microchim. Acta*, 183 (2016) 449–456.
- [25] J. Zolgharnein, M. Bagtash, T. Shariatmanesh, Simultaneous removal of binary mixture of Brilliant Green and Crystal Violet using derivative spectrophotometric determination, multivariate optimization and adsorption characterization of dyes on surfactant modified nano- $\gamma$ -alumina, *Spectrochim. Acta, Part A*, 137 (2015) 1016–1028.
- [26] J. Zolgharnein, M. Bagtash, N. Asanjarani, Hybrid central composite design approach for simultaneous optimization of removal of alizarin red S and indigo carmine dyes using cetyltrimethyl ammonium bromide-modified  $\text{TiO}_2$  nanoparticles, *J. Environ. Chem. Eng.*, 2 (2014) 988–1000.
- [27] Z.G. Peng, K. Hidajat, M.S. Uddin, Extraction of 2-hydroxyphenol by surfactant coated nanosized magnetic particles, *Korean J. Chem. Eng.*, 20 (2003) 896–901.
- [28] G. Absalan, M. Asadi, S. Kamran, L. Sheikhan, D.M. Goltz, Removal of reactive red-120 and 4-(2-pyridylazo) resorcinol from aqueous samples by  $\text{Fe}_3\text{O}_4$  magnetic nanoparticles using ionic liquid as modifier, *J. Hazard. Mater.*, 192 (2011) 476–484.
- [29] T. Saitoh, Y. Nakayama, M. Hiraide, Concentration of chlorophenol in water with sodium dodecylsulphate- $\gamma$ -alumina admicelles for high-performance liquid chromatographic analysis, *J. Chromatogr. A*, 972 (2002) 205–209.
- [30] X.L. Zhao, J.D. Li, Y.L. Shi, Y.Q. Cai, S.F. Mou, G.B. Jiang, Determination of perfluorinated compounds in wastewater and river water samples by mixed hemimicelle-based solid-phase extraction before liquid chromatography-electrospray tandem mass spectrometry detection, *J. Chromatogr. A*, 1154 (2007) 52–59.
- [31] J.D. Li, Y.Q. Cai, Y.L. Shi, S.F. Mou, G.B. Jiang, Determination of sulfonamide compounds in sewage and river by mixed hemimicelles solid-phase extraction prior to liquid chromatography-spectrophotometry, *J. Chromatogr. A*, 1139 (2007) 178–184.
- [32] J. Li, X. Zhao, Y. Shi, Y. Cai, S. Mou, G. Jiang, Mixed hemimicelles solid-phase extraction based on cetyltrimethyl ammonium bromide-coated nano-magnets  $\text{Fe}_3\text{O}_4$  for the determination of chlorophenols in environmental water samples coupled with liquid chromatography/spectrophotometry detection, *J. Chromatogr. A*, 1180 (2008) 24–31.
- [33] A. Ballesteros-Gomez, S. Rubio, Hemimicelles of alkyl carboxylates chemisorbed onto magnetic nano-particles: study and application to the extraction of carcinogenic polycyclic aromatic hydrocarbons in environmental water samples, *Anal. Chim.*, 81 (2009) 9012–9020.
- [34] D.K. Kim, Y. Zhang, W. Voit, K.V. Rao, M. Muhammed, Synthesis and characterization of surfactant-coated superparamagnetic monodispersed iron oxide nanoparticles, *J. Magn. Mater.*, 225 (2001) 30–36.
- [35] M. Bezerra, R. Santelli, E. Oliveira, L.S. Villar, L.A. Escalera, Response surface methodology (RSM) as a tool for optimization in analytical chemistry, *Talanta*, 76 (2008) 965–977.
- [36] S.L.C. Ferreira, R.E. Bruns, E.G.P. da Silva, W.N.L. dos Santos, C.M. Quintella, J.M. David, J.B. de Andrade, M.C. Breitenkreitz, I.C.S.F. Jardim, B.B. Neto, Statistical designs and response surface techniques for the optimization of chromatographic systems, review, *J. Chromatogr. A*, 1158 (2007) 2–14.
- [37] S.L.C. Ferreira, R.E. Bruns, H.S. Ferreira, G.D. Matos, J.M. David, G.C. Brandao, E.G.P. da Silva, L.A. Portugal, P.S. dos Reis, A.S. Souza, W.N.L. dos Santos, Box-Behnken design: an alternative for optimization of analytical methods, *Anal. Chim. Acta*, 597 (2007) 179–186.

- [38] J. Zolgharnein, A. Shahmoradi, J.B. Ghasemi, Comparative study of Box–Behnken, central composite, and Doehlert matrix for multivariate optimization of Pb (II) adsorption onto *Robinia* tree leaves, *J. Chemom.*, 27 (2013) 12–20.
- [39] P. Panneerselvam, N. Morad, K.A. Tan, Magnetic nanoparticle ( $\text{Fe}_3\text{O}_4$ ) impregnated onto tea waste for the removal of nickel (II) from aqueous solution, *J. Hazard. Mater.*, 186 (2011) 160–168.
- [40] S.I. Park, J.H. Kim, J.H. Lim, C.O. Kim, Surface-modified magnetic nanoparticles with lecithin for applications in biomedicine, *Curr. Appl. Phys.*, 8 (2008) 706–709.
- [41] R.D. Waldron, Infrared spectra of ferrites, *Phys. Rev.*, 99 (1955) 1727–1735.
- [42] K. Can, M. Ozmen, M. Ersoz, Immobilization of albumin on aminosilane modified superparamagnetic magnetite nanoparticles and its characterization, *Colloids Surf. B*, 71 (2009) 154–159.
- [43] J. Zolgharnein, A. Shahmoradi, P. Zolgharnein, S. Amani, Multivariate optimization and adsorption characterization of As(III) removal by using *Fraxinus* tree leaves, *Chem. Eng. Commun.*, 203 (2016) 210–223.
- [44] A.F. Barbosa, M.G. Segatelli, A.C. Pereira, A. de Santana Santos, L.T. Kubota, P.O. Luccas, C.R.T. Tarley, Solid-phase extraction system for Pb(II) ions enrichment based on multiwall carbon nanotubes coupled on-line to flame atomic absorption spectrometry, *Talanta*, 71 (2007) 1512–1519.
- [45] K.Y. Foo, B.H. Hameed, Insights into the modeling of adsorption isotherm systems, *Chem. Eng. J.*, 156 (2010) 2–10.
- [46] Y. Liu, Y.J. Liu, Biosorption isotherms, kinetics and thermodynamics, *Sep. Purif. Technol.*, 61 (2008) 229–242.
- [47] F. Gimbert, N. Morin-Crini, F. Renault, P.-M. Badot, G. Crini, Adsorption isotherm models for dye removal by cationized starch-based material in a single component system: error analysis, *J. Hazard. Mater.*, 157 (2008) 34–46.
- [48] K.V. Kumar, K. Porkodi, F. Rocha, Isotherms and thermodynamics by linear and non-linear regression analysis for the sorption of methylene blue onto activated carbon: comparison of various error functions, *J. Hazard. Mater.*, 151 (2008) 794–804.
- [49] J. Zolgharnein, T. Shariatmanesh, N. Asanjarani, A. Zolanvari, Doehlert design as optimization approach for the removal of Pb(II) from aqueous solution by *Catalpa Speciosa* tree leaves: adsorption characterization, *Desal. Wat. Treat.*, 53 (2015) 430–445.
- [50] B. Volskey, Sorption and Biosorption, BV Sorbex Inc., Montreal, Canada, 2003.
- [51] S. Moharami, M. Jalali, Removal of phosphorus from aqueous solution by Iranian natural adsorbents, *Chem. Eng. J.*, 223 (2013) 328–339.
- [52] R.K. Gautam, A. Mudhoo, M.C. Chattopadhyaya, Kinetic, equilibrium, thermodynamic studies and spectroscopic analysis of Alizarin Red S removal by mustard husk, *J. Environ. Chem. Eng.*, 1 (2013) 1283–1291.
- [53] R.K. Gautam, A. Mudhoo, G. Lofrano, M.C. Chattopadhyaya, Biomass-derived biosorbents for metal ions sequestration: adsorbent modification and activation methods and adsorbent regeneration, *J. Environ. Chem. Eng.*, 2 (2014) 239–259.
- [54] B.K. Nandi, A. Goswami, M.K. Purkait, Adsorption characteristics of brilliant green dye on kaolin, *J. Hazard. Mater.*, 161 (2009) 387–395.
- [55] V.S. Mane, P.V. Vijay Babu, Studies on the adsorption of Brilliant Green dye from aqueous solution onto low-cost NaOH treated saw dust, *Desalination*, 273 (2011) 321–329.
- [56] M.S. Ur Rehman, M. Munir, M. Ashfaq, N. Rashid, Adsorption of Brilliant Green dye from aqueous solution onto red clay, *Chem. Eng. J.*, 228 (2013) 54–62.
- [57] V.S. Mane, I.D. Mall, V.C. Srivastava, Use of bagasse fly ash as an adsorbent for the removal of brilliant green dye from aqueous solution, *Dyes Pigm.*, 73 (2007) 269–278.
- [58] Z. Wang, L.S. Zhang, Z.Q. Jing, Removal of brilliant green from aqueous solution using diatomite-attapulgite composite nano-size adsorbent, *Key Eng. Mater.*, 419–420 (2009) 525–528.